

NUMERICAL INVESTIGATION OF SHORT ELLIPTICAL TWISTED TUBE FOR REDUCED FOULING RATE IN STEAM CRACKING FURNACES.

*B. Indurain^{1,2}, F. Beaubert¹, D. Uystepruyst¹, S. Lalot¹ and M. Couvrat²

¹ LAMIH UMR CNRS 8201, Polytechnic University Hauts-de-France, 59300, Valenciennes, France.
bruce.indurainyurricelqui@uphf.fr (corresponding author)

² Manoir Industries, 27108, Val de Reuil Cedex, Pitres, France

ABSTRACT

In the steam cracking industry of natural gas or naphtha, fouling of tubular heat exchangers by cokes is one of the biggest issues regarding yields of valuable product and life span of the tubes composing the furnace. Coke build up on the tubes wall and this growing carbonaceous layer has two major negative effects: 1) it increases pressure drop and 2) reduces heat transfer from the tube wall to the processed fluid. Increasing wall shear stress yields higher friction forces at the wall of the tube which could reduce the coking rate. Previous studies prove that minor change of tubes cross section can both enhance wall shear stress and heat transfer by generating a swirling decaying flow. Using the open-source CFD software OpenFOAM, this study numerically investigates wall shear stress and pressure drop performances of swirl decaying flow generated by different elliptical cross-section twisted tube. One of the objectives is to determine if minor modifications of tube geometry can generate swirling flow which could enhance wall shear stress at a reduce pressure drop penalty. For a Reynolds number ranging from 10,000 to 100,000, it is shown that the investigated geometries could enhance heat transfer by 90% at an increased pressure drop of 128% which yields a Performance Evaluation Criterion (PEC) of 1.44. The comparison between the performances of the different geometries is carried out using a newly defined PEC based on the bulk temperature, along with the usual PEC.

INTRODUCTION

Steam cracking of naphtha and ethane produces about 85% of olefins made in the world, such as light olefins (ethylene, propylene, butene...) and aromatics [1]. The cracking reaction takes place within the tubes of the steam cracking furnaces at very high temperatures (above 1000 K) and produces the aforementioned products but also cokes on the wall of the tubes [2, 3]. This growing carbonaceous layer has several negative effects. First, coke build up decreases the cross-sectional area of

the gas flow resulting in higher pressure drop and loss of ethylene selectivity [4]. Secondly, the low thermal conductivity of cokes weakens the heat transfer from the tube wall to the process gas. Consequently, the heat input is raised to counteract the increased heat transfer resistance, leading to higher tube metal temperature (TMT) and still higher coking rate. Eventually, either due to an excessive pressure drop over the reactor or due to metallurgical constraints of the reactor tube alloy, production needs to be halted to decoke the reactor [5]. For obvious economics reasons coking rate must be slowed down. To that end, metallurgy developments of tubes [6,7] or three-dimensional reactor designs are used to enhance heat transfer, resulting in lower wall temperatures and/or higher wall shear stress and so to reduce coking rates as deduced from the well known Ebert and Panchal model (see e.g. [8]). Designs can be divided into two classes based on the physical reason of heat transfer: increased internal surface area or enhanced mixing.

Van Goethem et al. [9] numerically studied heat transfer and pressure drop of air flow in several heat transfer enhancers and among them there were straight and helical internally finned tube. For Reynolds numbers from 80,000 to 350,000, they reported that these increased surface technologies respectively enable an average increase in heat transfer of 51% and 66% compared to a straight tube yet at the expense of an average increased pressure drop of 67% and 92%. The better heat transfer performance of the helically finned tube is linked to its ability to generate a swirling flow and thus improving the mixing of the gas which leads to a more effective and more homogeneous heating of the process gas.

Swirling flow increases mixing in the fluid core section and results in increased shear stress at the wall. The studies conducted by Torigoe et al. [10] and Györffy et al. [11] focused on the heat transfer and pressure drop performances of a single start internally ribbed tube called Mixing Element Radiant Tube (MERT) patented

by Kubota in 1995 (see www.kubotamaterials.com.products/mert.html for a brief description). They found with the latest version of the MERT that the heat transfer is improved by up to 40% while the pressure drop is increased by up to 210%.

Although heat transfer is enhanced with the previous technologies, this is at the cost of a tremendous pressure drop increase. This drawback is mainly due to the added material at the tube surface. However, swirling flows could be generated by other means, such as deforming the tube shape as with the Swirl Flow Tube (SFT) developed by Technip [12, 13]. Van Goethem et al. [9] have experimentally and numerically studied this design of tube. The increased mixing is obtained by changing the shape of the tube from a straight to a small amplitude helical tube. Their results showed that for Reynolds numbers ranging from 30,000 to 120,000, the SFT can achieve a good balance between enhanced heat transfer and improved pressure drop with a 33% increase for both. Those results prove that a mere modification of the tube geometry could lead to a power efficient swirling flow.

Tubes with elliptical cross-sections have been widely studied and some of those researches focused on the heat transfer and pressure drop performances of twisted elliptical tube. Tan et al. [14] conducted a parametric study of a twisted elliptical tube and they reported that this kind of tube geometry offers an excellent Performance Evaluation Criterion (PEC) as defined by Webb and Eckert [15] within the studied Reynolds number range with the highest PEC reaching 1.725. It can also be concluded from their study that the greater the aspect ratio of the ellipse the higher the PEC and this is also true with the twist pitch of the tube but up to given value. This latest result shows that continuous swirling flow can become less efficient if it is maintained over a too long distance. Thus, after reaching a fully developed state, the swirling flow should decay and not increase pressure drop further.

This paper presents some results of a numerical investigation on the heat transfer and pressure drop performance of a developing swirling flow generated by a short length twisted tube with elliptical cross-section (SETET) and decaying downstream of the SETET in a tube with a circular cross-section. Several configurations of the SETET are studied in order to find the configuration which provides the highest heat transfer enhancement at the lowest pressure drop increase.

2. SHORT ELEMENT OF TWISTED ELLIPTICAL TUBE

The numeric test bench for the simulations consists of a tube composed of different elements. First of all, there is a twisted elliptical tube (TET) whose hydraulic diameter D_h is defined as:

$$D_h = 4 \frac{A}{E} \quad (1)$$

The twist operation of the elliptical cross-section consists in both a translation over a distance P and a 2π rotation along the tubes axis. The length of the TET is $L_{TET} = 20D_h$ and its inlet is considered as the origin of the axis coordinate ($z^* = 0$). Upstream of the TET there are two different elements, a transition tube and a tube with a circular cross-section. The latter has the same hydraulic diameter of the TET and has a length $L_{up} = 40D_h$. The purpose of this tube is to achieve a developed flow before entering the TET. The transition tube is used to have a smooth transition between the circular and the elliptical cross-section tubes over a length $L_{tr} = 4D_h$. Downstream of the TET, the same elements as upstream are used but the length of the tube with a circular cross-section is $L_{down} = 32D_h$ so that the total length of the test bench is $L = 100D_h$. L_{TET} is only one fifth of L , that is why the TET is renamed here as SETET. The computational domain can be seen on figure 1.

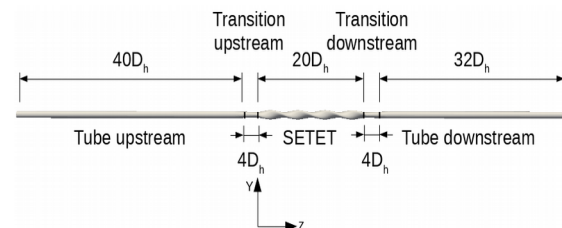


Fig. 1. Sketch of the numeric test bench with $P = 10D_h$.

The geometric parameter of this study is the twist pitch P and the aspect ratio of the ellipse c . As it can be seen in table 1 the twist pitch P for a given aspect ratio is tested.

Table 1. Tested geometric parameters with c the aspect ratio of the ellipse

Cases	P (m)	c
Case 1-1	$20D_h$	0.6
Case 1-2	$10D_h$	0.6
Case 1-3	$5D_h$	0.6

For every case five different Reynolds numbers (Re) are tested, they range from 10,000 to 100,000 and Re is defined as:

$$Re = \frac{\rho U_b D_h}{\mu} \quad (2)$$

3. SET UP OF THE NUMERICAL SIMULATIONS

The simulations are performed using the open source CFD software OpenFOAM. OpenFOAM is an open source object oriented numerical simulation toolkit developed in C++ and released under GPL license by the OpenFOAM®Foundation [16]. As no experimental data are yet available with the investigated tube configuration, a part of the numerical study conducted by Tang et al. [17] on the heat transfer and pressure drop performance of the flow in a twisted tube with elliptical cross-section was reproduced in this study.

3.1 Test case of Tang et al. [17]

The parameters of the elliptical cross-section are the ellipse major and minor axis which are respectively $a=0.024$ m and $b=0.015$ m. The numerical test bench, as shown on figure 2, is composed by a TET and two straight tubes with an elliptical cross-section upstream and downstream of the TET. The hydraulic diameter of the TET is given by Tang et al. to be $D_h=0.02$ m, and the twist pitch is $P=10D_h$. Ultimately, the length of the TET is $L=4P$.

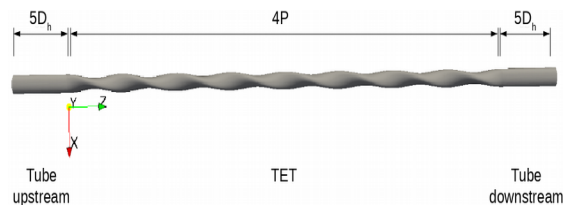


Fig. 2. Numeric test bench used by Tang et al. [17]

3.2. Boundary conditions and numerical schemes

The flow is considered steady, incompressible, turbulent with heat transfer and the flowing fluid is water. Considering the boundary conditions, a constant bulk velocity U_b based on the desired Reynolds number is imposed at the inlet along with a constant temperature $T_0=300$ K. A constant wall temperature $T_w=350$ K is imposed, and a no-slip condition is applied for the velocities. At the outlet, a constant pressure is imposed while null fluxes for the velocity and the temperature are set.

The different components of the governing equations (continuity, momentum and energy) are discretized using a second order bounded linear UPWIND scheme. The pressure-velocity linked equation are solved using the SIMPLE algorithm. A $k-\omega$ SST turbulence model with a Low-Re approach is used to reproduce the numerical work of Tang et al. [17]. At the inlet, the value of the turbulent kinetic energy k is set with the turbulent intensity and the specific dissipation rate ω is determined with the calculated value of k and the turbulent mixing length of the case. The corresponding formulas along with the governing equations can be found in Robertson et al. [18]. At

the outlet, a null flux boundary condition is imposed for both turbulent quantities and fixed values are imposed at the wall.

3.3. Validation of the numerical procedure

To quantify the pressure drop Δp along the TET, the friction factor coefficient f is used and is defined as:

$$f = 2 \frac{\Delta p D_h}{\rho U_b^2 L} \quad (3)$$

The heat transfer along the TET is quantified using the Nusselt number (Nu) defined as:

$$Nu = \frac{h D_h}{\lambda} \quad (4)$$

Heat transfer is calculated using a thermal energy balance between the inlet and outlet of the TET and the Nusselt number can be rewritten as:

$$Nu = \frac{\dot{m} c_p (\bar{T}_o - \bar{T}_i)}{\pi \lambda L T_{LMTD}} \quad (5)$$

where:

$$T_{LMTD} = \frac{\bar{T}_o - \bar{T}_i}{\ln \left(\frac{T_w - \bar{T}_o}{T_w - \bar{T}_i} \right)} \quad (6)$$

The results of the comparison between the simulations of the present study and the experimental data of Tang et al. [17] are shown in table 2. It can be observed that the maximum differences between the results of the simulations and the results from Tang et al. for Nu and f are respectively 6.3% and 5.2%. Those differences are sufficiently small to consider that the adopted numerical procedure is suitable to correctly predict heat transfer and pressure drop of a swirling flow generated by a twisted tube with elliptical cross-section. Therefore, this numerical procedure is adopted to study the different geometric configurations of SETET presented in table 1.

Table 2. Comparison between the results from the simulations of the present study and the experimental data from Tang et al [17].

Re	20,000	18,000	16,000	14,000
f_{Tang} [17]	0.0282	0.0294	0.0305	0.0322
f	0.0268	0.0279	0.0298	0.0311
Rel. dev	5.0%	5.2%	2.2%	3.2%
Nu_{Tang} [17]	102.2	93.7	85.9	77.4
Nu	95.7	90.8	83.0	78.3
Rel. dev	6.3%	3.1%	3.4%	1.1%

4. NUMERICAL SIMULATIONS OF THE SETET

The same numerical configuration as in the validation process of part 3 is kept here. However,

the working fluid is now air and the thermodynamic properties used are summed up in table 3. One assumption is that, within the given range of encountered temperatures, the thermodynamic properties are kept constant.

Table 3. Thermodynamic properties of air at T=300 K [19]

c_p (J/kgK)	1006
λ (W/mK)	0.024
μ (Pa.s)	1.91e-5
ρ (kg/m ³)	1.205

Although the numerical procedure has been validated, a mesh independent test study with case 1-1 is undertaken to ensure that the results of the simulations are not mesh sensitive.

4.1. Mesh independence test

The meshing process is achieved by using cfMesh, an open source meshing software developed by Dr. Franjo Juretic [20]. Three different cartesian unstructured meshes were tested with a refined mesh close to the wall of the tube consisting in 11 additional mesh layers. The three meshes from the finest to the coarsest are noted mesh 1, mesh 2 and mesh 3 and they respectively have 10,890,272, 7,632,400 and 5,330,459 cells. Mesh 2 is obtained with the same meshing parameters used for the validation case.

The Grid Convergence Index (GCI) method developed by Roache [21] is adopted here to conduct the mesh independence test. It is a generalization of the Richardson extrapolation and it provides a uniform measure of convergence for grid refinement studies. The GCI value represents the resolution level and how much the solution approaches the asymptotic value and is defined as:

$$GCI_i = 1.25 \frac{e_{i+1} - e_i}{e_i (r^\alpha - 1)} \quad (7)$$

where the grid refinement ratio r in this study is $r=1.43$ and α is computed as follows [21]:

$$\alpha = \frac{\ln\left(\frac{e_1 - e_2}{e_2 - e_3}\right)}{\ln(r)} \quad (8)$$

For the sake of clarity, the GCI method is not described here but can be found in [21,22]. Both global and local quantities are investigated with the GCI method. The global quantities are the friction factor f and the Nusselt number Nu . The local quantities are averaged values in a plane located in $z^*=34$ and they are the skin friction coefficient C_f and the bulk temperature T_b respectively defined as:

$$C_f = 2 \frac{\tau_w}{\rho U_b^2} \quad (9)$$

and

$$T_b = \frac{1}{U_b A} \int_A T u_z dA \quad (10)$$

The results of the grid refinement study are summarized in table 4 and it can be noticed that the GCI between mesh 1 and 2 is lower than the GCI between mesh 2 and 3 except for the Nusselt number but the GCI is still low. Therefore, the results of the simulations are less prone to change between mesh 1 and mesh 2. Furthermore, it is computationally less expensive to run simulations with mesh 2, thus this latest mesh was chosen to perform all the other simulations for the parametric study.

Table 4. Order of accuracy and Grid Convergence Index (GCI) for several flow quantities and for the three meshes.

	α	GCI ₂ (%)	GCI ₁ (%)
f	7.5	3.1	0.21
Nu	2.4	0.28	1.1
C_f	2.95	1.44	0.5
T_b	2.6	0.35	0.14

5. RESULTS AND DISCUSSION

5.1. Flow field

For the three cases, the swirling flow is generated in the same way. As the flow progresses through the SETET it acquires a tangential velocity component due to the geometry curvature. However, the lower the twist pitch of the SETET the greater the curvature and therefore the higher the intensity of the swirling flow as it can be seen on figure 3. In a cross-section of the SETET located at $z^*=10$, which corresponds to half the length of the twisted tube, the maximum dimensionless azimuthal velocity U_θ^* has been calculated for case 1-1, 1-2 and 1-3 and is respectively of 0.10, 0.28 and 0.53. As the twist pitch decreases, the maximum dimensionless tangential velocity increases significantly which leads to a greater mixing of the fluid, a longer flow path and an improved heat exchange between the swirling flow and the wall of the tube. In those same cross-sections, the mean deviation angle of the flow calculated between the tube axial direction and the flow velocity vector for the three cases is respectively of 9.2°, 16.9° and 24.5°. Again, the lower the twist pitch, the higher the mean deviation angle. This means that the wall of the twisted tube could deflect more efficiently the axial flow yielding to an intense swirling motion.

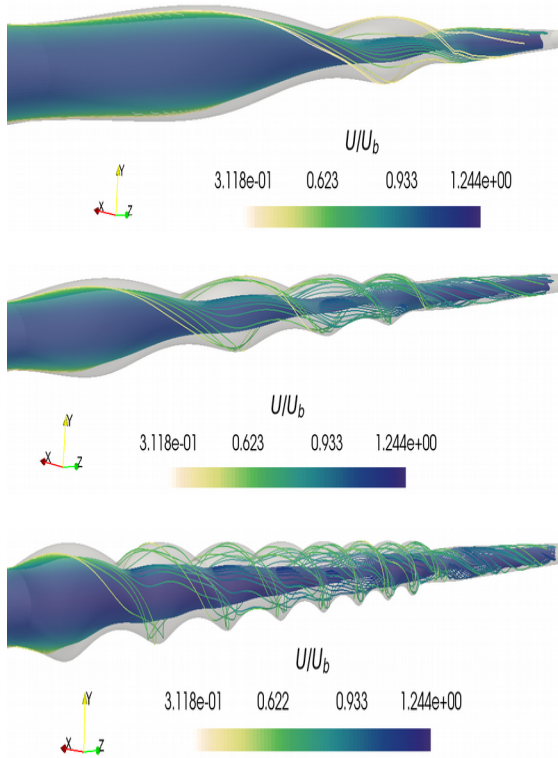


Fig. 3. Swirling flow in the different SETET. Case 1-1 (top), case 1-2 (middle) and case 1-3 (bottom) are all at Re=100,000.

In order to quantify the intensity of the swirling flow, a specific quantity is usually adopted and defined by Kitoh [23] as the swirl number S:

$$S = \frac{\int_0^R r^2 u_\theta u_z dr}{R \int_0^R r u_z^2 dr} \quad (11)$$

The evolution of S from $z^*=0$ to $z^*=51$ and for the three different cases at the highest Reynolds number is shown on figure 4, where the vertical bars delimitate the different phase of the swirling flow as discussed in the following. It must be noticed that there are three major phases: 1) from $z^*=0$ to $z^*=20$, the generation and development of the swirling flow, 2) at $z^*=20$ the transition between the SETET and the exit tube with circular cross-section where there is a huge drop of the swirl number and 3) from $z^*=24$ to $z^*=51$, the decay of the swirling flow. In phase 1, between all of the three cases, there are large difference of swirl numbers and the slopes are also greatly different from one another. The sharpest slope is achieved with case 1-3 meaning that the swirling flow is rapidly developing inside this SETET. For every case, there is a dramatic drop of the swirl number at $z^*=20$, caused by the end of the curved geometry and the rather sharp transition between an elliptical and a circular cross-section. Moreover, the higher the swirl number, the larger the drop of S.

Besides, it could also be observed that whatever length the SETET of case 1-1 might be, it will never generate a swirling flow whose S is as

high as the intensity of the SETET of case 1-2 after $10D_h$ or of case 1-3 after $5D_h$. In addition, if only one twist pitch of every SETET is considered, it must also be noticed that the shorter the length of P, the greater the value of S.

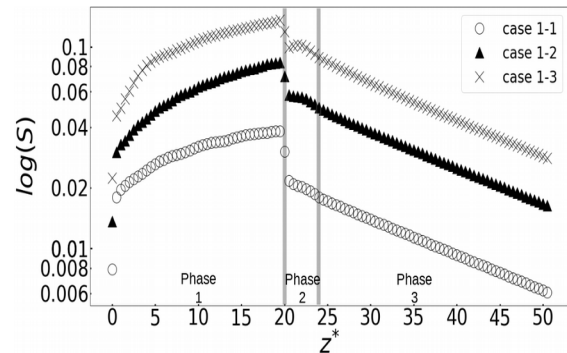


Fig. 4. Evolution of the swirl number along the TET and downstream for the cases 1-1, 1-2 and 1-3 at Re=100,000.

Ultimately, because of the logarithmic scale, it is easily observable that all of the three swirling flows have the same decay in phase 3. The calculation of the slope or decay rate of case 1-1 to 1-3 gives respectively a decay rate of 0.04, 0.041 and 0.042. This specific behavior of the swirling flows is shown on figure 5, where the graph has been built as follows. The evolution of S from case 1-3 is used and the last value of S at $z^*=51$ is stored. Then, the closest value of S from case 1-2 to the latest stored S is found and added to the graph along with the subsequent values of S from case 1-2 and the latest value is stored. Then this operation is done once more between case 1-1 and 1-2.

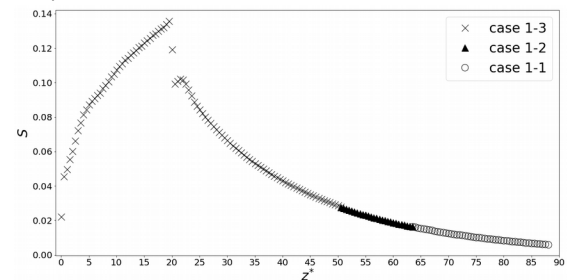


Fig. 5. Reconstruction of the Swirl number from the three cases at Re=100,000.

Although the pitch of the SETET has a tremendous influence on the development of the swirling flow, it has very little regarding its decay. Figure 5 also illustrates that with case 1-3, the swirling flow could last over almost almost $70D_h$ after the SETET.

5.2. Pressure Drop

The swirling flow generated by the three SETET are greatly different as previously seen on figure 3 and 4. Hence it is important to study the evolution of the friction factor with the Reynolds number, depending on the SETET. Figure 6 features the friction factor ratio between the

SETET (f) and a straight tube (f_p) where f_p is calculated with the correlation from Pethukov:

$$f_p = (0.79 \ln(R_e) - 1.64)^{-2} \quad (11)$$

while f is computed by using Eq. (3) between $z^*=0$ and $z^*=51$.

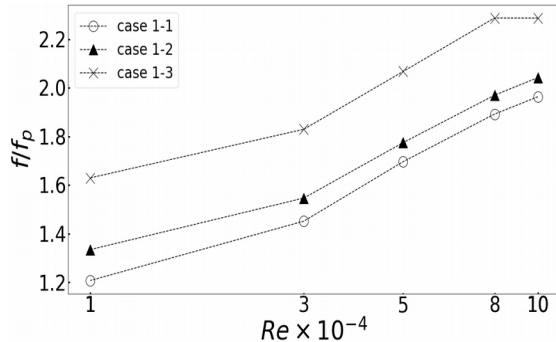


Fig. 6. Evolution of f/f_p with Re for cases 1-1 to 1-3.

The transition between the elliptical cross-section and the circular cross-section might cause a large pressure drop due to a sudden change of the flow topology as depicted with the sharp variation of the swirl number in phase 2 on figure 4. Pressure loss of case 1-2 are higher than case 1-1 but are in the same range especially compared to case 1-3 where the pressure drop are tremendously higher.

5.3. Heat Transfer

The amount of heat exchanged between the fluid and the wall depends also greatly on the swirling flow. The calculation of the bulk temperature T_b with Eq. (8) and its evolution from $z^*=0$ to $z^*=51$ for every cases, as seen on figure 7, gives information on how effective the swirling flow is to transport the heat from the wall to the bulk flow.

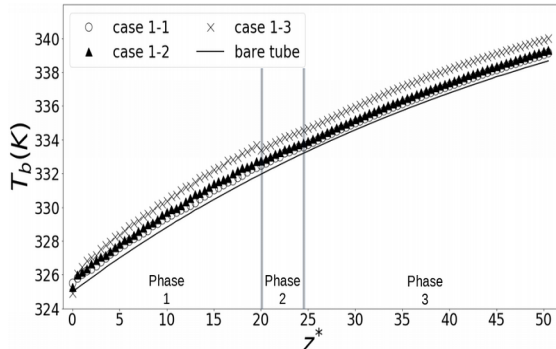


Fig. 7. Evolution of T_b along the TET and downstream for cases 1-1 to 1-3 and for the straight tube at $Re=100,000$.

The swirling flow generated by the SETET of case 1-3 is more effective at increasing the bulk temperature than the two other SETET. Although this increase is not really high, it means that the swirling flow enables a more effective heat transfer between the wall of the tube and the flow. As a consequence, for a given heat flux at the wall of the tube, the increased heat transfer will have two

major effects in steam cracking furnaces. First of all, it will result in a diminution of the wall temperature and according to the coking model of Plehiers [24] yield a lower coking rate. Secondly, because of the imparted swirling motion, it will lead to a more uniform radial temperature distribution which in turn decreases secondary reactions which also participate to the coke formation [25, 26]. Furthermore, more heat is transported by the rotating fluid as shown on figure 8 which displays the ratio between the global heat transfer obtained with an enhanced geometry (Nu) and the heat transfer obtained in a straight tube (Nu_p) where Nu_p is calculated with the correlation of Gneilinsky:

$$Nu_p = \frac{\frac{f_p}{8} (R_e - 1000) Pr}{1 + 12.7 \left(\frac{f_p}{8}\right)^{0.5} Pr^{0.6666-1}} \quad (12)$$

where Pr is the Prandtl number and is defined as:

$$Pr = \frac{\mu C_p}{\lambda} \quad (13)$$

The Nusselt number is calculated from Eq. (5) and the heat balance is done between $z^*=0$ and $z^*=51$.

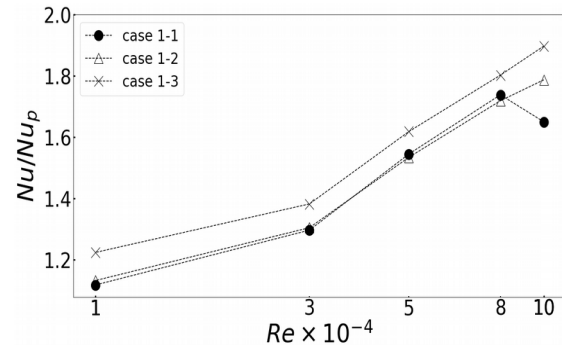


Fig. 8. Evolution of Nu/Nu_p with Re for cases 1-1 to 1-3.

It can be observed that both cases 1-1 and 1-2 provide approximately the same heat transfer enhancement and are both below the heat transfer enhancement of case 1-3. All the SETET are efficient at enhancing heat transfer and the improvement grows with the Reynolds number, except for case 1-1 at $Re=100,000$ where there is a sudden drop of Nu/Nu_p . The improved heat transfer and the relatively low pressure drop increase from the twisted tube is of particular interest for the steam cracking industry because again it leads to a lower TMT and provided that the coke deposition occurs at the wall where the temperatures are the highest to a lower coking rate [13, 26, 27]. Similarly, considering the Ebert and Panchal model, the enhanced heat transfer of the SETET leads to a diminution of the deposition term by increasing the heat transfer coefficient in the thermal boundary layer and by reducing the wall

temperature thus leading to a diminution of the fouling rate [8].

Even though every investigated SETET generate a swirling flow which increases pressure drop, it also enhances significantly the heat transferred between the wall and the flowing fluid. To quantify the energetic efficiency of the SETET, the Performance Evaluation Criterion (PEC), proposed by Webb et al. [15] is used here and is defined as:

$$PEC = \frac{Nu/Nu_p}{\sqrt[3]{f/f_p}} \quad (14)$$

The evolution of the PEC for the different cases is shown on figure 9.

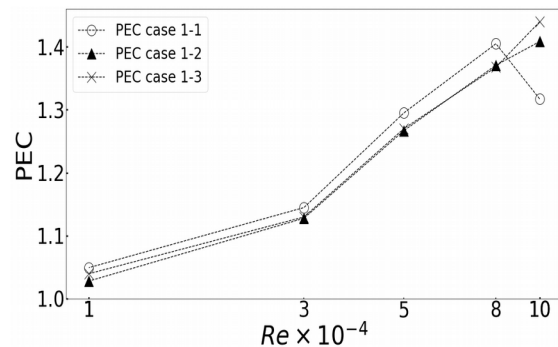


Fig. 9. Evolution of PEC with Re for cases 1-1 to 1-3.

Although the SETET of case 1-3 provides better heat transfer performance at the cost of a higher pressure drop than the two other SETET, it can be observed that all the studied geometries have approximately the same PEC with a slightly higher values for the SETET with the greatest twist pitch. Considering that the SETET of case 1-3 generates the most intense swirling flow which increases both the wall shear stress and the heat transfer at the same PEC as the two other SETET, it is concluded that this SETET is the most interesting studied configuration.

6. THE BULK TEMPERATURE RELATED PEC

In the steam cracking industry, the temperature of the processed gas is a prime parameter to achieve a better selectivity in highly valuable products (ethylene, propylene...). The higher the bulk temperature, the better the selectivity and also the lower the radial temperature gradient and the lower the coking rate [25]

It was seen in section 5.3, on figure 7 that every configuration of SETET generates a swirling flow which yields higher T_b along z^* than in a turbulent flow in a straight tube. Thus, the required length of tube in cases 1-1 to 1-3 to reach the same bulk temperature as the one at the end of a straight tube, here at $z^*=51$, is shorter. This length is denoted as L_{eq} and new calculations of the friction factor and the Nusselt number with respectively

Eqs. (3) and (4) between $z^*=0$ and $z^*=L_{eq}$ are performed to determine the PEC associated with this reduction of tube material to achieve the same T_b as in a straight tube. This new number is denoted PEC_b .

The values of L_{eq} for every cases is shown on table 5 and from this table it is clear that the SETET from case 1-3 achieve the same T_b as in a straight tube within a dramatically shorter distance. Thus the total length of the tube with the SETET of case 1-3 could be reduced to a maximum of nearly 65% at $Re=80,000$ and to a minimum of 17% at $Re=100,000$. It is also surprising to observe such an increase of L_{eq} between these two Reynolds numbers from case 1-3. It must also be noticed that the two other SETET are quite inefficient at reducing the length of tube required to obtain the same T_b as in a straight tube.

Table 5. L_{eq} obtained with cases 1-1 to 1-3 at every Reynolds number.

Re	10^5	8.10^4	5.10^4	3.10^4	1.10^4
Case 1-1 L_{eq}	47.5 D_h	48 D_h	48 D_h	48 D_h	34.5 D_h
Case 1-2 L_{eq}	46.5 D_h	47 D_h	47 D_h	46 D_h	35 D_h
Case 1-3 L_{eq}	42.5 D_h	18 D_h	19 D_h	20.5 D_h	29.5 D_h

The evolution of the PEC_b for the different cases is shown on figure 10.

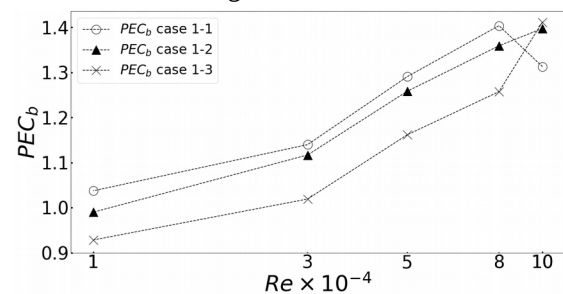


Fig. 10. Evolution of PEC_b with Re for cases 1-1 to 1-3.

From the latest figure it can be observed that the PEC_b of case 1-2 is below 1 for $Re=10,000$ and for case 1-3 is below 1 for the two lowest Reynolds numbers, meaning that this solution causes more pressure drop than heat transfer enhancement. However, at higher Reynolds number the PEC_b becomes higher than 1 and thus the generated swirling flows are energetically efficient.

CONCLUSION

This work presents a numerical study of different geometry of short length twisted elliptical tube (SETET) used to induced a swirling flow, followed by a transition tube and a tube with a circular cross-section. Three configurations of SETET, whose length remain the same, are studied

and the tested parameter is the twist pitch P of the SETET. The Reynolds number range from 10,000 to 100,000 and from the results of the study the following conclusions can be drawn:

- With this kind of configuration the swirling flow could be decomposed into three phases: a developing, transitioning and decaying.
- The SETET with the shortest twist pitch features the highest swirl number S and the best heat transfer enhancement at a given Re but also the highest pressure loss.
- The better heat transfer that leads to a higher bulk temperature is expected to yield a lower coking rate according to the coking model of Plehiers [24].
- The PEC of the three cases are in the same range and are above 1.

According to this last result, it can be concluded that minor modification of tube geometry or shape could generate a swirling flow which enhances heat transfer at a relative low pressure drop penalty and which might also reduce significantly the coking rate.

It was also shown in the last section of this study that the swirling flow generated by the SETET with the lowest twist pitch can achieve the same bulk temperature reached at the end of a straight tube within a shorter distance. Therefore, tube manufacturers could save money by using this configuration of SETET and by shortening their tubes. Furthermore, more heat is transferred with the generated swirling flow, meaning that the temperature at the wall is lower and therefore that the coking rate could be reduced thus extending run lengths and have less frequent shutting down for decoking operations

Nevertheless, the large drop of swirl intensity in phase 2 is detrimental for the swirling flow and future work aims at creating another transition which could reduce this swirl intensity gap. Furthermore, to reduce the pressure drop another parametric study with the aspect ratio c is expected to be undertaken with the most interesting configuration of SETET investigated namely the case 1-3.

ACKNOWLEDGMENT

The authors are extremely grateful for the financial support provided by Manoir Industries within the scope of the CIFRE convention 2017/1437.

NOMENCLATURE

A	area of tube cross-section, m^2
a	major axis of the ellipse, m
b	minor axis of the ellipse, m
C_f	skin friction coefficient, dimensionless

c	aspect ratio of the ellipse, (b/a) , dimensionless
c_p	specific heat capacity, J/kgK
D_h	hydraulic diameter, m
E	circumference of tube cross-section, m
e	quantity to evaluate for the GCI
f	friction factor coefficient, dimensionless
h	heat transfer coefficient, W/m^2K
k	turbulent kinetic energy, J/kg
L	total length of the tested tube, m
\dot{m}	mass flow rate, kg/s
Nu	Nusselt number, dimensionless
P	twist pitch, m
Pr	Prandtl number, dimensionless
Re	Reynolds number, dimensionless
R	hydraulic radius, m
r	refinement ratio, dimensionless
S	Swirl number, dimensionless
T	temperature, K
TMT	tube metal temperature
U	fluid velocity, m/s
U_θ^*	dimensionless tangential velocity, (U_θ/U_b)
z^*	dimensionless axial position (z/D_h)
α	order of accuracy for the GCI, dimensionless
Δp	pressure drop, Pa
λ	thermal conductivity, W/mK
μ	dynamic viscosity, $Pa.s$
ρ	fluid density, kg/m^3
ω	specific dissipation rate, $1/s$
τ_w	wall shear stress, Pa

Subscripts

0	<i>inlet value</i>
b	bulk
down	downstream tube
eq	equivalent
LMTD	Logarithmic Mean Temperature Difference
i	inlet of SETET
o	outlet of SETET
p	straight tube
TET	twisted elliptical tube
tr	transition tube
up	upstream tube
w	wall
z	axial component
θ	tangential component

Superscripts

$-$	area averaged quantity
-----	------------------------

REFERENCES

- [1] T. Ren, M.K. Patel and K. Blok, Steam cracking and methane to olefins: Energy use, CO_2 emissions and production costs, *Energy*, 33 (2008): 817-833

- [2] K. Sundaram and G. Froment, Kinetics of coke deposition in the thermal cracking of propane, *Chemical Engineering Science*, 34, (1979): 635-644
- [3] P. Plehiers, G. Reyniers and G. Froment, Simulation of the Run Length of an Ethane Cracking Furnace, *Industrial & Engineering Chemistry Research*, 29 (1990): 636-641
- [4] K. Kolmetz, J. Kivlen, J. Gray, C. Sim and C. Soyza, Advances in cracking Furnace Technology, Refining Technology Conference, Dubai Crown Plaza Hotel, 2002
- [5] L. Vandewalle, D. Van Cauwenberge, J. Dedeysne, K. Van Geem and G. Marin, Dynamic simulation of fouling in steam cracking reactors using CFD, *Chemical Engineering Journal*, 329 (2017): 77-87
- [6] S. Symoens et al., State-of-the-art of Coke Formation during Steam Cracking: Anti-Coking Surface Technologies, *Industrial & Engineering Chemistry Research*, 57, 48 (2018): 16117-16136
- [7] N. Olahová et al., CoatAlloy Barrier Coating for Reduced Coke Formation in Steam Cracking Reactors: Experimental validation and Simulations, *Industrial & Engineering Chemistry Research*, 57, 3 (2018) :897-907
- [8] I. Wilson, E. Ishiyama and G. Polley, Twenty Years of Ebert and Panchal-What Next?, *Heat Transfer Engineering*, 38:7-8 (2017): 669-680
- [9] M. Van Goethem and E. Jelsma, Numerical and experimental study of enhanced heat transfer and pressure drop for high temperature applications, *Chemical Engineering Research and Design*, 92 (2014): 663-671
- [10] T. Torigoe, K. Hamada, M. Furuta, M. Sakashita, K. Otsubo and M. Tomita, Mixing Element Radiant Tube (MERT) improves cracking furnace performance, In: *Proceedings of the 11th Ethylene Producers Conference* (1999)
- [11] M. Györfy, M. Hineno, K. Hashimoto, S.H. Park, M.S. You, MERT performance and technology update, *AICHE Spring Meeting: Ethylene Producers Conference*, 20 (2009), Tampa Bay, USA
- [12] D. Van Cauwenberge, C. Schietekat, J. Floré, K. Van Geem and G. Marin, CFD-based design of 3D pyrolysis reactors: RANS vs. LES, *Chemical Engineering Journal*, 282 (2015): 66-76
- [13] C. Schietekat, M. Van Goethem, K. Van Geem and G. Marin, Swirl flow tube reactor technology: An experimental and computational fluid dynamics study, *Chemical Engineering Journal*, 238 (2014): 56-65
- [14] X. Tan, D. Zhu, G. Zhou and L. Zeng, Experimental and numerical study of convective heat transfer and fluid flow in twisted oval tubes, *International Journal of Heat and Mass Transfer*, 55 (2012): 4701-4710
- [15] R. Webb and E. Eckert, Application of rough surfaces to heat exchanger design, *International Journal of heat and Mass Transfer*, 15 (1972): 1647-1658
- [16] C.J. Greenshield, CFD direct Ltd, OpenFOAM User Guide version 4.0, ©2011-2016, OpenFOAM Foundation Ltd
- [17] X. Tang, X. Dai and D. Zhu, Experimental and numerical investigation of convective heat transfer and fluid flow in twisted spiral tube, *International Journal of Heat and Mass Transfer*, 90 (2015): 523-541
- [18] E. Robertson, V. Choudhury, S. Bhushan and D. Walters, Validation of OpenFOAM numerical methods and turbulence models for incompressible bluff body flows, *Computers and Fluids* 123 (2015): 122-145
- [19] Y. Çengel and J. Cimbala, *Fluid mechanics: fundamental and applications*, New York, NY 10020, McGraw-Hill (2006)
- [20] Juretic F. *cfMesh User Guide (v1.1)*, 2015
- [21] P.J Roache, Perspective: A Method for Uniform Reporting of Grid Refinement Studies, *Journal of Fluids Engineering*, 116 (1994): 405-413
- [22] M. Ali, C. Doolan and V. Wheatley, Grid convergence study for two-dimensional simulation of flow around a square cylinder at a low Reynolds number, *7th International Conference on CFD in the Minerals and Process Industries* (2009)
- [23] O. Kitoh, Experimental study of turbulent swirling flow in a straight pipe, *Journal of Fluid Mechanics*, 225 (1991): 445-479
- [24] P. Plehiers, D. Froment, Firebox simulation of olefin units, *Chemical Engineering Communications*, 80 (1989): 81-99
- [25] K. Van Geem, G. Heynderickx and G. Marin, Effect of Radial Temperature Profiles on Yields in Steam Cracking, *AICHE Journal*, 50, 1 (2004): 173-183
- [26] C. Schietekat, D. Van Cauwenberge, K. Van Geem and G. Marin, Computational Fluid Dynamics-Based Design of Finned Steam Cracking Reactors, *AICHE Journal*, 60 (2014), No. 2: 794-808
- [27] L. Vandewalle, D. Van Cauwenberge, J. Dedeysne, K. Van Geem and G. Marin, Dynamic simulation of fouling in steam cracking reactors using CFD, *Chemical Engineering Journal*, 329 (2017): 77-87